J|A|C|S
ARTICLES
Published on Web 09/26/2006

Solid-State NMR of a Paramagnetic DIAD-Fe^{II} Catalyst: Sensitivity, Resolution Enhancement, and Structure-Based Assignments

Gwendal Kervern,[†] Guido Pintacuda,[†] Yong Zhang,[‡] Eric Oldfield,[‡] Charbel Roukoss,[§] Emile Kuntz,[§] Eberhardt Herdtweck,[∥] Jean-Marie Basset,[§] Sylvian Cadars,[†] Anne Lesage,[†] Christophe Copéret,[§] and Lyndon Emsley*[,†]

Contribution from the Laboratoire de Chimie, UMR 5182 CNRS−ENS Lyon, Ecole Normale Supérieure de Lyon, 46 Allée d'Italie, 69364 Lyon Cedex 07, France, Departments of Chemistry and Biophysics, University of Illinois at Urbana-Champaign, 600 South Mathews Avenue, Urbana, Illinois 61801, Laboratoire de Chimie Organométalliaque de Surface, UMR 9986 CNRS−ESCPE Lyon, 43 bd du 11 Novembre 1918, 69616 Villeurbanne Cedex, France, and Department Chemie, Lehrstuhl für Anorganische Chemie, Technische Universität München, Lichtenbergstrasse 4, D-85747 Garching bei München, Germany

Received June 6, 2006; E-mail: lyndon.emsley@ens-lyon.fr

Abstract: A general protocol for the structural characterization of paramagnetic molecular solids using solid-state NMR is provided and illustrated by the characterization of a high-spin Fe^{II} catalyst precursor. We show how good NMR performance can be obtained on a molecular powder sample at natural abundance by using very fast (>30 kHz) magic angle spinning (MAS), even though the individual NMR resonances have highly anisotropic shifts and very short relaxation times. The results include the optimization of broadband heteronuclear (proton-carbon) recoupling sequences for polarization transfer; the observation of single or multiple quantum correlation spectra between coupled spins as a tool for removing the inhomogeneous bulk magnetic susceptibility (BMS) broadening; and the combination of NMR experiments and density functional theory calculations, to yield assignments.

Introduction

Solid-state NMR has proven to be an effective tool for the characterization of noncrystalline organic samples, including diamagnetic organometallic complexes.[1] In combination with techniques such as EXAFS and IR, solid-state NMR can provide unique insights into the analysis of the structures of heterogeneous catalysts and a description of surface chemistry processes.[2] In many recent examples, steps and mechanisms of surface reactions could be inferred from the detection of reaction intermediates and end products.[3] Many catalysts, however, depend on the use of paramagnetic metal ions.[4] NMR potentially provides a method for determining paramagnetic shifts and relaxation rates, which are direct probes of the molecular geometries and of the electronic structures in such compounds. However, to date, solid-state NMR studies of solid paramagnetic organometallic complexes have been hindered by the existence of large orientation-dependent paramagnetic shifts, as well as paramagnetically enhanced nuclear relaxation, both of which hamper data acquisition and spectral assignment. This makes solid-state NMR of paramagnetic molecules somewhat challenging, and there have been only a rather limited number of successful examples in the literature.[5−10] Traditionally, some of these problems are alleviated or circumvented by ^{13}C and ^{2}H labeling,[5,6] which provides a considerable spectral simplification, makes assignment easier, and, in the case of ^{2}H, opens a

[†] Laboratoire de Chimie, UMR 5182 CNRS−ENS Lyon.
[‡] University of Illinois.
[§] Laboratoire de Chimie Organométalliaque de Surface, CNRS−ESCPE Lyon.
[∥] Technische Universität München.

(1) (a) Schmidt-Rohr, K.; Spiess, H. W. *Multidimensional Solid-State NMR and Polymers*. Academic Press: London, 1994. (b) Laws, D. D.; Bitter, H.-M. L.; Jerschow, A. *Angew. Chem. Int. Ed.* **2002**, *41*, 3096−3129.
(2) (a) Chabanas, M.; Baudouin, A.; Coperet, C.; Basset, J. M.; Lukens, W.; Lesage, A.; Hediger, S.; Emsley, L. *J. Am. Chem. Soc.* **2003**, *125*, 492−504. (b) Le Roux, E.; Chabanas, M.; Baudouin, A.; de Mallmann, A.; Coperet, C.; Quadrelli, E. A.; Thivolle-Cazat, J.; Basset, J. M.; Lukens, W.; Lesage, A.; Emsley, L.; Sunley, G. J. *J. Am. Chem. Soc.* **2004**, *126*, 13391−13399. (c) Rataboul, F.; Baudouin, A.; Thieuleux, C.; Veyre, L.; Coperet, C.; Thivolle-Cazat, J.; Basset, J. M.; Lesage, A.; Emsley, L. *J. Am. Chem. Soc.* **2004**, *126*, 12541−12550. (d) Blanc, F.; Coperet, C.; Thivolle-Cazat, J.; Basset, J. M.; Lesage, A.; Emsley, L.; Sinha, A.; Schrock, R. R. *Angew. Chem. Int. Ed.* **2006**, *45*, 1216−1220.
(3) (a) Chabanas, M.; Quadrelli, E. A.; Fenet, B.; Coperet, C.; Thivolle-Cazat, J.; Basset, J. M.; Lesage, A.; Emsley, L. *Angew. Chem. Int. Ed.* **2001**, *40*, 4493−4496. (b) Lesage, A.; Emsley, L.; Chabanas, M.; Coperet, C.; Basset, J. M. *Angew. Chem. Int. Ed.* **2002**, *41*, 4535−4538.
(4) Cotton, F. A.; Wilkinson, G.; Murillo, C. A.; Bochmann, M. *Advanced inorganic chemistry*, 6th ed.; Wiley: New York, 1999.
(5) (a) Clayton, A. N.; Dobson, C. M.; Grey, C. P. *J. Chem. Soc., Chem. Commun.* **1990**, 72−74. (b) Brough, A. R.; Grey, C. P.; Dobson, C. M. *J. Chem. Soc., Chem. Commun.* **1992**, 742−743. (c) Heise, H.; Kohler, F. H.; Mota, F.; Novoa, J. J.; Veciana, J. *J. Am. Chem. Soc.* **1999**, *121*, 9659−9667. (d) Crozet, M.; Chaussade, M.; Bardet, M.; Emsley, L.; Lamotte, B.; Mouesca, J. M. *J. Phys. Chem. A* **2000**, *104*, 9990−10000.
(6) Liu, K.; Ryan, D.; Nakanishi, K.; Mcdermott, A. *J. Am. Chem. Soc.* **1995**, *117*, 6897−6906.
(7) (a) Liu, K.; Williams, J.; Lee, H. R.; Fitzgerald, M. M.; Jensen, G. M.; Goodin, D. B.; McDermott, A. E. *J. Am. Chem. Soc.* **1998**, *120*, 10199−10202. (b) Lee, H.; Polenova, T.; Beer, R. H.; McDermott, A. E. *J. Am. Chem. Soc.* **1999**, *121*, 6884−6894. (c) Lee, H.; de Montellano, P. R. O.; McDermott, A. E. *Biochemistry* **1999**, *38*, 10808−10813.

window for probing local conformational dynamics around the metal center.[7] The requirement though of a large number of ^{13}C and ^{2}H labeled samples for complete characterization limits the impact of this approach.

This latter limitation can be overcome by the use of samples containing natural isotopic abundance ^{13}C, as recently demonstrated by Ishii and co-workers,[9,10] where enhanced sensitivity and resolution were obtained by using very fast MAS, and rapid 2D heteronuclear correlation and dipolar-edited experiments could be used to assign ^{13}C and ^{1}H signals, at least in simple model compounds. Nevertheless, most of these advances have been restricted to paramagnetic centers possessing a small magnetic susceptibility (electron spin $S = {}^1/_2$) and/or isotropic.

Unfortunately, paramagnetic centers featuring a large spin, and thus a large electronic moment, together with a large susceptibility anisotropy are, by far, the most common in inorganic and bio-inorganic samples. In these cases, from an NMR perspective, the situation changes radically. First, a large electronic spin S greatly increases the anisotropy of the nuclear shifts, which is dominated by the dipolar coupling with the electronic moment, and grows proportionally to $S(S + 1)\gamma_I$ (where γ_I is the gyromagnetic ratio of the nuclear spin I).[11] Second, an anisotropic paramagnetic susceptibility tensor makes the electron−nuclear dipolar shift tensor nontraceless,[12] introducing new terms into the isotropic nuclear shift δ^{obs} observed under MAS. Thus, in addition to the orbital contribution (δ^{dia}), as commonly observed in diamagnetic molecules, and a Fermi contact term (δ^{fc}, the trace of the through-bond electron−nucleus coupling tensor),[13] δ^{obs} now consists of the so-called pseudocontact term (δ^{pc}, the trace of the electron−nuclear dipolar interaction)[14] and a bulk magnetic susceptibility (BMS) contribution (δ^{BMS}):

$$\delta^{obs} = \delta^{dia} + \delta^{fc} + \delta^{pc} + \delta^{BMS} \quad (1)$$

Since the BMS tensor for a crystallite is also anisotropic, the size of δ^{BMS} depends on the nuclear position in the crystallite.[15]

In most cases, when considering small metal complexes where nuclei are separated by only a few bonds from the paramagnetic center, δ^{pc} and particularly δ^{BMS} are only minor corrections and the hyperfine shifts are dominated by the contact contribution, δ^{fc}. However, due to the random distribution of the orientations of the crystallites in the sample, the bulk magnetic susceptibility (and thus δ^{BMS}) varies randomly in the powder, causing a distribution of magnetic fields, and therefore a broadening of the isotropic peaks of an MAS NMR spectrum.[15,16] This effect becomes the dominant source of spectral broadening for such systems, its contribution to the observed line width being potentially larger than the relaxation enhancement induced by the paramagnetic center.[17]

Scheme 1

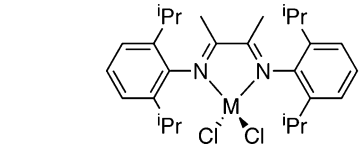

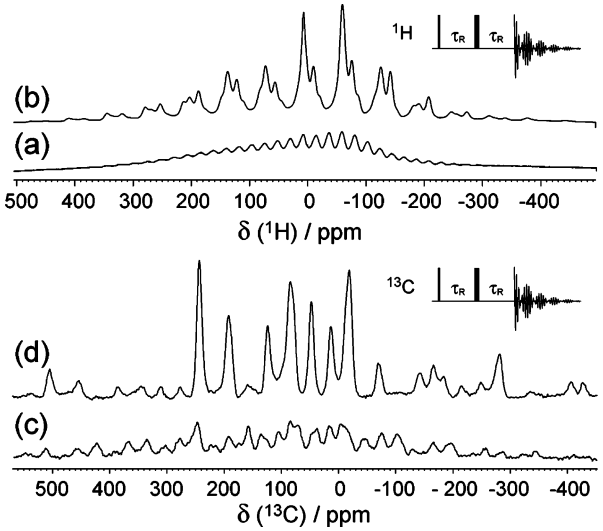

Figure 1. (a,b) ^{1}H and (c,d) ^{13}C MAS NMR spectra of **1** acquired at MAS frequencies of 11 kHz (a,c) and 33 kHz (b,d) (temperature: 303 K, B_0: 11.7 T). As T_2 relaxation may interfere with the comparisons, the same echo delay τ of 90 μs (equal, respectively, to 1 and 3 rotor periods) was used in all the experiments.

Here we present a strategy for characterizing, at natural abundance, a powdered molecular solid containing paramagnetic metal ions having large, anisotropic susceptibilities. We show how spectra free of BMS broadening can be obtained in short times and that they can be interpreted on the basis of a reference molecular structure, by combining multipulse and multidimensional NMR methods with quantum chemical calculations. The challenge is illustrated by the characterization of **1** (Scheme 1), a high-spin ($S = 2$) DIAD−Fe^{II} complex (DIAD: 2,3-dimethyl-1,4-[(2′,6′)-diisopropylphenyl]-*N*,*N*′-diazadiene) belonging to a new family of efficient polymerization catalysts.[18−20]

Results and Discussion

Sensitivity and Resolution Enhancement. Figure 1 shows the ^{1}H and ^{13}C NMR spectra of **1** acquired at 500 MHz, at MAS speeds of 11 and 33 kHz. As noticed by Ishii and co-workers,[10] sensitivity and resolution experience a spectacular enhancement under very high MAS. Despite this dramatic effect, fast sample

(8) (a) Heise, H.; Kohler, F. H.; Xie, X. L. *J. Magn. Reson.* **2001**, *150*, 198−206. (b) Heise, H.; Kohler, F. H.; Herker, M.; Hiller, W. *J. Am. Chem. Soc.* **2002**, *124*, 10823−10832. (c) Ziessel, R.; Stroh, C.; Heise, H.; Kohler, F. H.; Turek, P.; Claiser, N.; Souhassou, M.; Lecomte, C. *J. Am. Chem. Soc.* **2004**, *126*, 12604−12613. (d) Sporer, C.; Heise, H.; Wurst, K.; Ruiz-Molina, D.; Kopacka, H.; Jaitner, P.; Kohler, F.; Novoa, J. J.; Veciana, J. *Chem.−Eur. J.* **2004**, *10*, 1355−1365. (e) Jovanovic, T.; McDermott, A. *J. Am. Chem. Soc.* **2005**, *127*, 13816−13821.
(9) Ishii, Y.; Wickramasinghe, N. P.; Chimon, S. *J. Am. Chem. Soc.* **2003**, *125*, 3438−3439.
(10) Wickramasinghe, N. P.; Shaibat, M.; Ishii, Y. *J. Am. Chem. Soc.* **2005**, *127*, 5796−5797.
(11) Brough, A. R.; Grey, C. P.; Dobson, C. M. *J. Am. Chem. Soc.* **1993**, *115*, 7318−7327.
(12) Bertini, L.; Luchinat, C.; Parigi, G. *Prog. NMR Spectrosc.* **2002**, *40*, 249−273.
(13) Bertini, I.; Luchinat, C.; Parigi, G. *Solution NMR of paramagnetic molecules: applications to metallobiomolecules and models*. Elsevier: Amsterdam, London, 2001.
(14) Nayeem, A.; Yesinowski, J. P. *J. Chem. Phys.* **1988**, *89*, 4600−4608.
(15) Alla, M.; Lippmaa, E. *Chem. Phys. Lett.* **1982**, *87*, 30−33.
(16) (a) Schwerk, U.; Michel, D.; Pruski, M. *J. Magn. Reson., Ser. A* **1996**, *119*, 157−164. (b) Kubo, A.; Spaniol, T. P.; Terao, T. *J. Magn. Reson.* **1998**, *133*, 330−340.
(17) Banci, L.; Luchinat, C.; Bertini, I. *Nuclear and electron relaxation: the magnetic nucleus-unpaired electron*. VCH: Weinheim, 1991.
(18) (a) Gibson, V. C.; O'Reilly, R. K.; Reed, W.; Wass, D. C.; White, A. P. J.; Williams, D. J. *Chem. Commun.* **2002**, 1850−1851. (b) Gibson, V. C.; O'Reilly, R. K.; Wass, D. C.; White, A. P. J.; Williams, D. J. *Macromolecules* **2003**, *36*, 2591−2593.
(19) Bart, S. C.; Hawrelak, E. J.; Schmisseur, A.; Lobkovsky, E.; Chirik, P. J. *Organometallics* **2004**, *23*, 237−246.
(20) Shaver, M. P.; Allan, L. E. N.; Rzepa, H. S.; Gibson, V. C. *Angew. Chem. Int. Ed.* **2006**, *45*, 1241−1244.

rotation is not capable of averaging the anisotropy of the hyperfine interactions, even for nuclei with lower gyromagnetic ratios (^{13}C), so the signal intensity is still spread over hundreds of ppm into a large family of sidebands.

A. Bulk Magnetic Susceptibility (BMS) Broadening. Furthermore, the resonances appear much broader than those observed under similar conditions, for Cu^{II} or Mn^{II} complexes.[9,10] Especially in the case of the proton, this prevents the observation of any resolved peaks. This broadening cannot be explained by a paramagnetic relaxation enhancement. Indeed, in the absence of molecular motion, the paramagnetic center can only influence nuclear relaxation via electron relaxation (Solomon mechanism).[17] Average relaxation rates were measured for ^1H and ^{13}C signals: T_1's were found to be 1 ms for ^1H, 15 ms on average for ^{13}C (in the range between 7.1 ± 0.2 ms and 20.5 ± 2.5 ms), while values of 0.55 ms for ^1H and around 2 ms (ranging from 1.6 ± 0.3 ms to 2.5 ± 0.3 ms) for ^{13}C were found for T_2'. Reported correlation times for electronic fluctuations (τ_e) are on the order of 10^{-11} s for high-spin tetrahedral Fe^{II} complexes,[13] a time scale which agrees with the measured T_1's. However, the measured T_2' values indicate that more than a significant part of the line width observed in the ^{13}C spectrum is refocusable, a large portion of it being accounted for, potentially, by BMS inhomogeneous fields.

It has been shown that BMS broadening can be removed by observing zero quantum (ZQ) coherences between two coupled spins.[21] Since the ZQ coherence between two spins evolves at the frequency difference of their two shifts, and since the BMS shift is constant on the molecular scale, the BMS shift drops out of the ZQ shift. For example, $^{13}C-^{13}C$ ZQ coherences could be efficiently excited through homonuclear J couplings in ^{13}C-enriched lanthanide acetates.[21] However, a ZQ experiment is not the only way to obtain a spectrum free of inhomogeneous broadening: narrow spectra can be observed in *any* case where the generation of a coherence correlates different sites experiencing the same inhomogeneous field.[22] Any nQ−mQ correlation can feature a high-resolution projection (a "pseudo-ZQ spectrum") along a certain axis.[23] In this case, at natural abundance, we propose that BMS broadening can be removed by applying this idea to $^1H-^{13}C$ pairs. This corresponds to building up a "heteronuclear pseudo-ZQ spectrum" from an SQ−SQ correlation which may be obtained through the dipolar couplings between neighboring spins.

B. Heteronuclear Correlation Spectra. Unfortunately, a conventional CP experiment does not provide an efficient way to generate correlations between nuclear spins in a highly paramagnetic material, as can be seen in Figure 2, where we compare a CP MAS spectrum (Figure 2b) to a ^{13}C direct excitation experiment (Figure 2a). This is because, first, the very short ^1H T_1's impose strict limits on the transfer, which cannot exceed half a millisecond in length. Second, routinely available rf fields are unable to lock spins over the large bandwidths swept by the anisotropic shifts during a rotor cycle. Furthermore, the efficiency of the CP transfer at high MAS rates is penalized by the different nature of the network of the ^1H homonuclear dipolar couplings, as compared to the diamagnetic situation. That is,

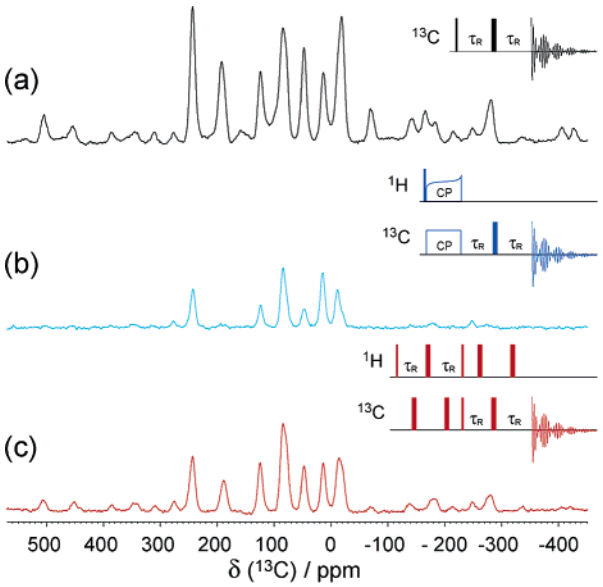

Figure 2. Comparison between ^{13}C MAS NMR spectra of **1**, obtained through direct carbon excitation using the sequence shown inset (a, black line), via CP (b, blue line; contact time: 500 μs) and via the modified TEDOR sequence (c, red line; recoupling time: 60 μs). Narrow and wide rectangles denote 90° and 180° pulses, respectively; τ_R represents the rotor period.

neighboring nuclei can experience significantly different paramagnetic shifts during a rotor cycle, even if their isotropic shifts are very similar.[11] This phenomenon decouples the flip−flop interaction between protons,[6] setting extremely narrow limits for the Hartman−Hahn condition. The simultaneous occurrence of large instantaneous offsets and of a sharp Hartman−Hahn condition prevent uniform CP transfer, with a resulting loss of efficiency.

To counter this problem, we developed a transfer sequence which does not suffer from these drawbacks. Figure 2 shows that the use of a simple heteronuclear recoupling sequence like TEDOR (transferred-echo, double resonance)[24,25] provides a broadband, offset-insensitive route to much more efficiently record 2D correlations on strongly paramagnetic signals. The pulsed nature of the sequence allows the use of higher ^1H and ^{13}C fields, and two rotor cycles for the transfer period at high spinning speeds ensure a transfer with optimal efficiency.[26] The result of using TEDOR, shown in Figure 2c, yields much more uniform transfers than the spectrum shown in Figure 2b from CP. Notably, several peaks are completely absent in the CP spectrum but are readily detectable in the TEDOR experiment. Although the coherent transfer mechanism behind the TEDOR scheme is generally less efficient than an adiabatic CP, elevated spinning speeds have also been shown to improve TEDOR transfers in diamagnetic solids,[27] and it has been observed at spinning speeds over 28 kHz that the insensitivity of TEDOR

(21) Spaniol, T. P.; Kubo, A.; Terao, T. *Mol. Phys.* **1999**, *96*, 827−834.
(22) Maudsley, A. A.; Wokaun, A.; Ernst, R. R. *Chem. Phys. Lett.* **1978**, *55*, 9−14.
(23) Sakellariou, D.; Brown, S. P.; Lesage, A.; Hediger, S.; Bardet, M.; Meriles, C. A.; Pines, A.; Emsley, L. *J. Am. Chem. Soc.* **2003**, *125*, 4376−4380.
(24) (a) Hing, A. W.; Vega, S.; Schaefer, J. *J. Magn. Reson.* **1992**, *96*, 205−209. (b) Saalwachter, K.; Graf, R.; Demco, D. E.; Spiess, H. W. *J. Magn. Reson.* **1999**, *139*, 287−301. (c) Saalwachter, K.; Graf, R.; Spiess, H. W. *J. Magn. Reson.* **1999**, *140*, 471−476.
(25) Saalwachter, K.; Graf, R.; Spiess, H. W. *J. Magn. Reson.* **2001**, *148*, 398−418.
(26) The pulse sequence presented in Figure 2c is a slightly modified version of the standard TEDOR, which lacks the final *z*-filter so that acquisition can be started right after the reconversion period on the ^{13}C channel. This alteration does not alter the quality of the resulting spectra on this system but allows a sizable shortening of the whole sequence, with the elimination of the final spin−echo and the relaxation losses associated with it.
(27) Schnell, I. *Prog. NMR Spectrosc.* **2004**, *45*, 145−207.

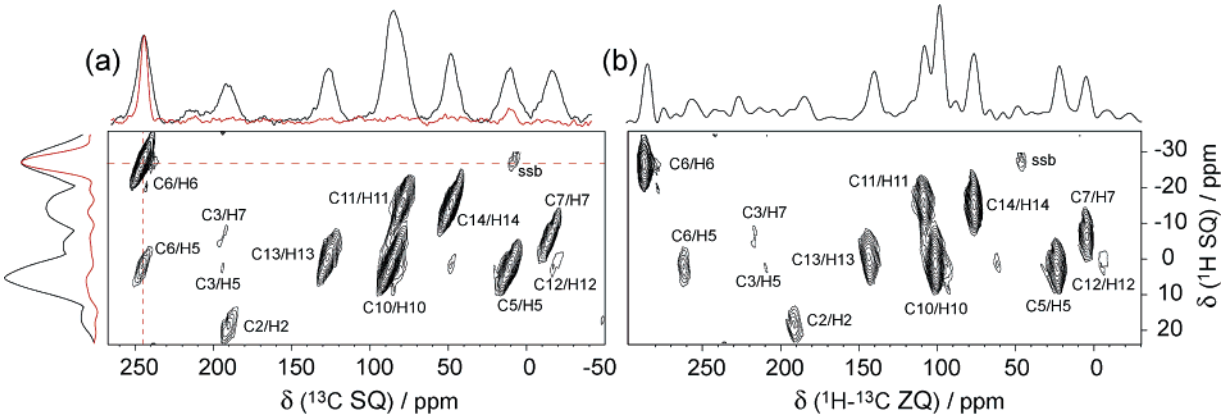

Figure 3. (a) 2D $^{1}H-^{13}C$ TEDOR of **1** (recoupling time: 60 μs). Displayed along the axes are the projections along f_2 and f_1 (black spectra) and the traces along f_2 and f_1 (red spectra), taken at the frequencies of 245.4 and −25.6 ppm, respectively, as indicated by the dashed red lines. (b) The same $^{1}H-^{13}C$ correlation as that in (a), after a shearing transformation was applied along f_2; displayed above is the projection onto f_2. Signals are labeled according to their assignment as discussed in the main text.

to RF homogeneity makes it superior to CP for amide ^{1}H to ^{15}N transfers.[28]

C. High-Resolution Correlation Spectra. The 2D version of the TEDOR experiment is shown in Figure 3a. The elongated shape of the signals is a clear signature of highly correlated inhomogeneous broadening. Although both projections along the ^{1}H and ^{13}C dimensions feature line widths of more than 10 ppm, any cross-section parallel to the ω_2 and ω_1 axes yields lines less than 6 ppm broad. All signals have a tilted profile with the same slope, which is unitary when the two axis scales are expressed in ppm. It is clear that a skew projection along this particular direction would substantially enhance the resolution. This projection *is* the pseudo-ZQ spectrum mentioned above.

This dimension is readily accessible (Figure 3b) if the 2D spectrum $S(\omega_1, \omega_2)$ is transformed into a sheared spectrum $S(\omega_1, \omega_2')$ where $\omega_2' = \omega_2 - \omega_1$. This can be obtained during processing, by applying a modified shearing transformation,[29] in which a first-order phase correction is applied to each row of the f_1 transformed data, the phase factor being the correspondent ω_1 *in ppm*.

The projection of the sheared spectrum onto the ω_2-axis yields a full spectrum where correlated inhomogeneous broadening, including all the BMS broadening, is completely eliminated; each line here possesses around a 5 ppm full width at half-height, corresponding to an improvement of more than a factor of 2 in line width as compared to the directly detected spectra. Note, of course, that there is no additional information in the sheared spectrum, which we only show here to clearly illustrate the principle.

Interestingly, a spectrum of the quality of that shown in Figure 3 can be acquired very rapidly. Short proton T_1 values are turned into an advantage, allowing increased repetition rates,[9] which are here only limited by the duty factor of the probe. The TEDOR spectra were acquired with a repetition time of 100 ms, to favor comparison with the CP results. In fact, the absence of decoupling and spin-lock fields enables the use of a repetition time as short as 10 ms for TEDOR, yielding a remarkably short overall time of 2.3 h for acquisition of a 2D spectrum of the same quality as the one displayed in Figure 3. Furthermore, aliasing in the indirect dimension has additional benefits, if t_1 is incremented by integer multiples of the rotor period (i.e., if the spectral width in the indirect dimension is chosen equal to a fraction of the spinning speed). First, each member of the numerous sideband families are wrapped around into single signals, with a corresponding increase in sensitivity. Second, strongly shifted signals are rolled into a narrow spectral width in the indirect dimension, reducing the number of increments needed for maximal resolution; their isotropic chemical shift (the centerband position) can then be easily and unambiguously calculated from two spectra acquired at different, suitably chosen, spinning speeds.[30]

In summary then, at a spinning speed of 33 kHz, a total of 16 k scans for 16 time points can typically be acquired in 7 h (2 h using a repetition time of 10 ms). The resolution enhancement provided by the correlated broadening, combined with the efficient performance of the TEDOR sequence, permits us to detect 14 different cross-peaks and to record with high confidence the chemical shifts of 12 distinct carbon and 9 distinct proton sites. The lines from two additional carbon sites (presumably quaternary) can be located by comparison between the 1D spectra obtained by direct ^{13}C excitation and by TEDOR (Figure 2).

Spectral Assignment. Experimental support for resonance assignment can be provided by $^{1}H-^{13}C$ dipolar editing experiments,[9,31] in which the carbon spectrum is acquired after a REDOR-type recoupling sequence where $^{1}H-^{13}C$ dipolar couplings are switched on or off by 180° pulses applied on the ^{1}H channel, as shown in Figure 4 both for a 1D and a 2D case. Depending on the number and the dynamics of the coupled protons, a carbon signal experiences differential dephasing (CH_2 > CH > CH_3 > quaternary).[32]

Only four signals appear strongly affected in the dephased TEDOR (Figure 4b), suggesting their assignment to CH groups; the other five intense peaks in the 2D correlation conserve their amplitude despite the proton recoupling, consistent with the behavior of methyl groups. Finally, the two signals which appear only in the 1D spectrum (Figure 4a) and do not show any $^{1}H-$

(28) Morcombe, C. R.; Paulson, E. K.; Gaponenko, V.; Byrd, R. A.; Zilm, K. W. *J. Biomol. NMR* **2005**, *31*, 217−230.
(29) Ernst, R. R.; Bodenhausen, G.; Wokaun, A. *Principles of nuclear magnetic resonance in one and two dimensions*. Clarendon: Oxford, 1987.
(30) Dunn, A. J.; Sidebottom, P. J. *Magn. Reson. Chem.* **2005**, *43*, 124−131.
(31) McElheny, D.; De Vita, E.; Frydman, L. *J. Magn. Reson.* **2000**, *143*, 321−328.
(32) De Vita, E.; Frydman, L. *J. Magn. Reson.* **2001**, *148*, 327−337.

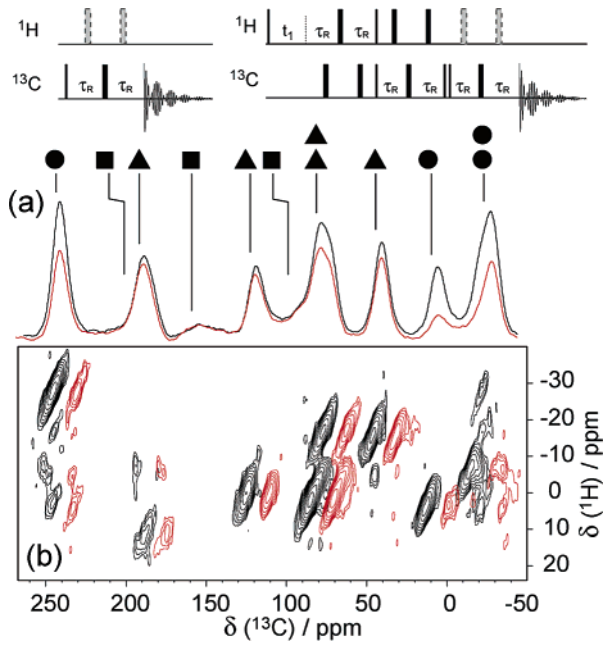

Figure 4. Comparison between NMR spectra of **1** acquired without (colored lines) and with (gray lines) ^{1}H dipolar filter editing (shaded pulses): (a) ^{13}C MAS and (b) TEDOR. Signals are labeled according to the correspondent carbon type: quaternary (■), methine (●), and methyl (▲). Narrow and wide rectangles denote 90° and 180° pulses, respectively; τ_R represents the rotor period. The contours of the edited experiment (b, red lines) have been shifted 15 ppm upfield in the ^{1}H dimension to allow an easier comparison.

^{13}C correlation are also insensitive to proton recoupling, confirming their assignment to quaternary centers.

The details of the spin multiplicities, and thus of the identity of a carbon spin, inferred from these measurements are compatible with the molecular formula but obviously do not provide enough insight into such a complex spectrum to allow more detailed assignments.

To do this, we investigated the possible uses of quantum chemical calculations in assisting the assignment process. Paramagnetic shifts are sensitive probes of electronic structure and geometry, and when the 3D structure of a complex is known, the chemical shifts can be quite accurately predicted by evaluating the spin density distribution.[33] For example, we have recently found that hyperfine effects can be reproduced both in solution and in the solid-state in small paramagnetic model systems, as well as in metalloproteins, in solution.[34−36]

We therefore determined the X-ray crystallographic structure of **1** (Table 1), which features C_s symmetry (Figure 5). The iron center is involved in a distorted tetrahedral coordination[37] which drives a bending of the two aromatic rings out of the diimine plane, causing different separations between the isopropyl groups above and below the metal center and, therefore, a global nonequivalence of the two sides of the rings.

Table 1. Crystallographic Data for Compound **1**

formula	$C_{28}H_{40}Cl_2FeN_2$
formula weight	531.37
crystal system	orthorhombic
space group	*Pnma* (no. 62)
a, Å	12.6185(2)
b, Å	21.3367(3)
c, Å	10.4310(1)
V, Å^3	2808.41(7)
Z	4
T, K	173
d_{calcd}, g cm^{-3}	1.257
μ, mm^{-1}	0.745
no. of independent reflections	2646
no. of observed reflections ($I > 2\sigma(I)$)	2504
no. of data/restraints/parameters	2646/0/234
$R1/wR2^a$ ($I > 2\sigma(I)$)	0.0330/0.0704
$R1/wR2^a$ (all data)	0.0358/0.0716
GOF^a (on F^2)	1.167

^{a} $R1 = \Sigma(||F_o| - |F_c||)/\Sigma|F_o|$; $wR2 = \{\Sigma[w(F_o^2 - F_c^2)^2]/\Sigma[w(F_o^2)^2]\}^{1/2}$; GOF $= \{\Sigma[w(F_o^2 - F_c^2)^2]/(n - p)\}^{1/2}$.

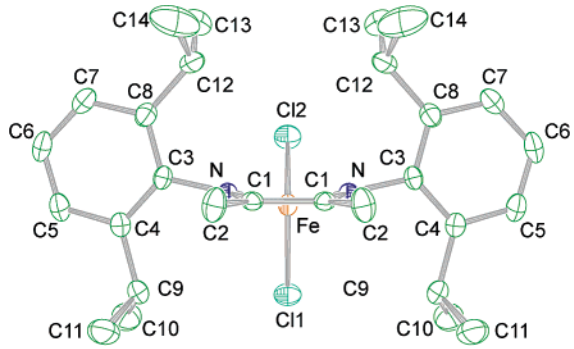

Figure 5. ORTEP view of **1** with 30% probability ellipsoids, and the atom labeling scheme. Hydrogens atoms were omitted for clarity.

This distortion produces, respectively, 14 carbon and 10 proton magnetically nonequivalent nuclei, a number fully compatible with the total number of the observed resonances (12 and 9, respectively).

We investigated the electronic structure of **1** using density functional theory,[43,44] as described in the Experimental Section. The calculation yields information on the Fermi contact spin densities at the nuclei; if pseudocontact terms can be neglected (which is generally the case, as shown previously[33−34,46]), these values are directly proportional to the NMR hyperfine shifts.

(33) Mao, J. H.; Zhang, Y.; Oldfield, E. *J. Am. Chem. Soc.* **2002**, *124*, 13911−13920.
(34) Zhang, Y.; Sun, H. H.; Oldfield, E. *J. Am. Chem. Soc.* **2005**, *127*, 3652−3653.
(35) Zhang, Y.; Gossman, W.; Oldfield, E. *J. Am. Chem. Soc.* **2003**, *125*, 16387−16396.
(36) (a) Zhang, Y.; Mao, J. H.; Godbout, N.; Oldfield, E. *J. Am. Chem. Soc.* **2002**, *124*, 13921−13930. (b) Zhang, Y.; Mao, J. H.; Oldfield, E. *J. Am. Chem. Soc.* **2002**, *124*, 7829−7839.
(37) The $FeCl_2$ and FeN_2 planes are perfectly orthogonal; as a consequence of a folding of the chelate ring about the NN vector, the iron lies 0.538 Å out of the diimine plane in the direction of Cl(2).
(38) The correlation is significantly worse if only the ^{1}H shifts are taken into account, since the calculation uncertainties are mostly comparable to the absolute values of the shifts. Not surprisingly, the spin density of the unpaired electrons is higher at the carbon sites as compared to the proton sites, resulting in smaller hyperfine contributions to the ^{1}H spectrum.
(39) Bart, S. C.; Hawrelak, E. J.; Schmisseur, A. K.; Lobkovsky, E.; Chirik, P. J. *Organometallics* **2004**, *23*, 237−246.
(40) Sandrini, P. L.; Mantovani, A.; Crociani, B.; Uguagliati, P. *Inorg. Chim. Acta* **1981**, *51*, 71−80.
(41) Hediger, S.; Meier, B. H.; Kurur, N. D.; Bodenhausen, G.; Ernst, R. R. *Chem. Phys. Lett.* **1994**, *223*, 283−288.
(42) (a) Data Collection Software for Nonius κ-CCD devices; Delft, The Netherlands, 2001. (b) Otwinowski, Z.; Minor, W. *Methods Enzymol.* **1997**, *276*, 307ff. (c) Altomare, A.; Cascarano, G.; Giacovazzo, C.; Guagliardi, A.; Burla, M. C.; Polidori, G.; Camalli, M. SIR92. *J. Appl. Crystallogr.* **1994**, *27*, 435−436. (d) *International Tables for Crystallography*; Wilson, A. J. C., Ed.; Kluwer Academic Publishers: Dordrecht, The Netherlands, 1992; Vol. C, Tables 6.1.1.4, 4.2.6.8, and 4.2.4.2. (e) Spek, A. L. *PLATON, A Multipurpose Crystallographic Tool*; Utrecht University: Utrecht, The Netherlands, 2001. (f) Sheldrick, G. M. *SHELXL-97*: Universität Göttingen: Göttingen, Germany, 1998.
(43) (a) Becke, A. D. *Phys. Rev. A* **1988**, *38*, 3098−3100. (b) Becke, A. D. *J. Chem. Phys.* **1993**, *98*, 5648−5652.
(44) Pople, J. A. et al. *Gaussian 03*, revision C.02; Gaussian, Inc.: Wallingford, CT, 2004.
(45) Wachters, A. J. H. *J. Am. Chem. Soc.* **1970**, *52*, 1033−1036. Basis sets were obtained from http://www.emsl.pnl.gov/forms/basisform.html.

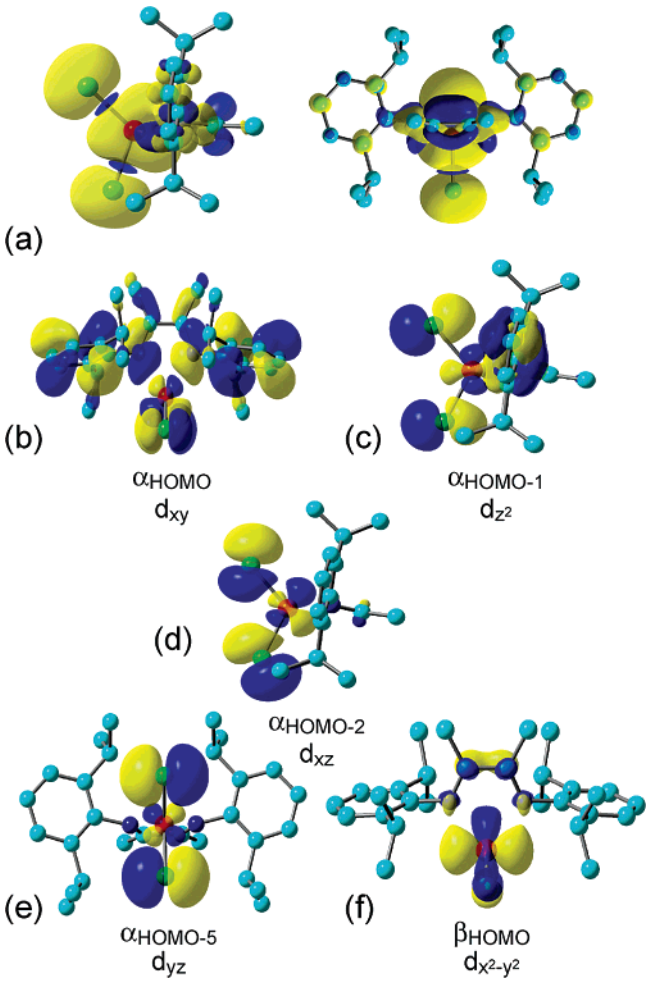

Figure 6. (a) Spin density for **1**, (contour at ±0.0004 au), superimposed to two views of the molecular structure (atom color scheme: Fe, red; Cl, green; C, cyan; N, blue). (b−f) Isosurface representation of the frontier molecular orbitals for **1**: (b) α_{HOMO}, (c) α_{HOMO-1}, (d) α_{HOMO-2}, (e) α_{HOMO-5}, (f) β_{HOMO}. Contour values are ±0.02, 0.03, 0.03, 0.03, 0.04 au, respectively.

As shown in Figure 6a, the major spin densities reside on iron; residual spin densities are located on the chlorine ligands, and, to a lesser extent, on the whole aryl-diimine, due to the highly conjugated nature of this system. Consistent with this picture, the calculated Mulliken spin density ($\rho_{\alpha\beta}$) of iron is 3.65 au, similar to that found in deoxy myoglobin ($S = 2$), 3.80 au.[33]

DFT methods also enable accurate calculations of the diamagnetic contribution to the total shifts. Alternatively, this component can be directly accessed experimentally, if an isostructural complex of a diamagnetic ion is available. Reference diamagnetic shifts were here obtained by recording and assigning the NMR spectra of the Zn^{II} analogue **2**. The results are summarized in Table 2. Note that the agreement between diamagnetic shifts calculated by DFT and the experimental values measured for **2** is very good; this means that the two datasets would contribute similarly when used to calculate the total paramagnetic shifts for **1**.

A route for a global assignment can immediately be envisaged by comparing the results of the calculation to the observed NMR shifts. In fact, the editing measurements of Figure 4 significantly

Table 2. Experimental and Predicted ^{13}C and ^{1}H NMR Shifts (ppm) in the Iron and Zinc Complexes **1** and **2**[a]

	δ^{obs}(**2**)	δ^{obs}(**1**)	δ^{dia}_{calc}(**1**)	δ^{dia}_{calc}(**1**) + δ^{fc}_{calc}(**1**)	δ^{obs}(**2**) + δ^{fc}_{calc}(**1**)
C1	172.5		164	3	11.5
C2	20.8	195	−7	362	389.8
C3	137.8	170	143	162	156.8
C4	139.4	155	139	146	146.4
C5	124.5	10.9	116	12	20.5
C6	126.2	245.4	118	239	247.2
C7	123.7	−15.5	116	−66	−57.3
C8	139.4	105	140	50	49.4
C9	28.6		13	−84	−68.6
C10	25.4	86.5	0	83	108.4
C11	23.3	78.9	−5	68	96.8
C12	27.4	−18.8	12	−42	−26.6
C13	24.5	126.6	−5	106	135.5
C14	24.9	47.7	0	26	50.9
H2	2.6	79.2	−3	−29	−23.4
H5	6.5	3.2	4	21	23.5
H6	6.5	−25.6	5	−23	−20.5
H7	6.7	−5.4	4	6	8.7
H9	2.7		−2	−4	0.7
H10	1.3	2.2	−3	−1	3.3
H11	0.4	−15.2	−4	−4	0.4
H12	3.1	1.7	−3	−4	2.1
H13	1.5	0.2	−4	−2	3.5
H14	1.3	−14.8	−3	−1	3.3

[a] Uniform experimental uncertainties were of the order of ±0.5 ppm.

constrain the choice for the assignment of the experiment to the theory; the proposed combination reported in Table 2 is the one that minimizes the squared deviation of calculated and experimental shifts within each group of signals with a given carbon multiplicity. According to this assignment, only one quaternary carbon (C_1) and one CH group (C_9-H_9, the isopropyl substituent of the phenyl rings, which sits closest to the metal center) escape detection. All the other one-bond correlations are observed in the 2D TEDOR. Consistently, in this way the weaker, most broad signals are assigned to $^{1}H-^{13}C$ spin pairs located closer to the metal ($C_{12}-H_{12}$, C_2-H_2). We expect that the fact that the C_9-H_9 peak is absent is mainly due to the short relaxation time of the H_9 proton, which is the closest proton to the metal, and which does therefore not allow sufficient time to transfer magnetization to the carbon. As shown in Figure 7, the correlation between calculated and experimental chemical shifts for **1** is generally good (theory-versus-experiment correlation coefficient $R = 0.88$). The outlier is the methyl group closest to the metal (the C_2-H_2 resonance), which if excluded from the correlation results in $R = 0.97$, a slope of 0.96, an intercept of 2.9 ppm, and an rms error of 20 ppm (or 7% of the whole experimental range of 271 ppm).

To try to improve upon these results, we next investigated a dimer model calculation, since H_2 has short contacts with the two Cl atoms (2.9 and 3.2 Å, in the X-ray structure) in the neighboring molecule. The dimer calculation does significantly reduce the errors of the proposed C_2 and H_2 NMR shifts, by 66 and 33 ppm (see Table S7), respectively, and improves the overall correlation from $R = 0.88$ to $R = 0.93$. The desirability of incorporating additional metal centers was observed previously in calculations on another paramagnetic complex,[34] which required the use of a nine-metal complex cluster. However, calculations on clusters larger than the dimer (1442 basis functions) are prohibitively expensive with current resources and are likely to only improve the results for C_2/H_2 (note that, for signals other than C_2/H_2, R is still 0.97 in the dimer calculation, as in the monomer calculation) and further exac-

(46) Wilkens, S. J.; Xia, B.; Weinhold, F.; Makley, J. L.; Westler, W. M. *J. Am. Chem. Soc.* **1998**, *120*, 4806−4814.

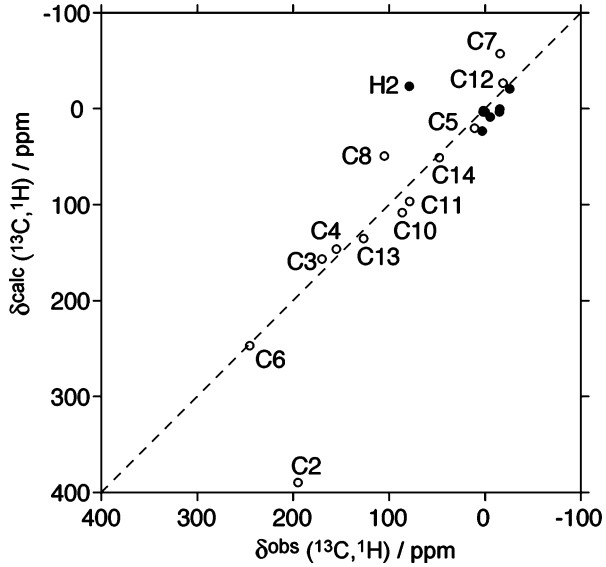

Figure 7. Experimental δ^{obs} vs calculated δ^{calc} ^{13}C (open symbols) and ^{1}H (filled symbols) NMR shifts of **1**. Uniform experimental uncertainties were of the order of ±0.5 ppm

erbate the problem of visualizing the orbitals and spin densities described below. So, here and below we focus solely on the monomer results (e.g., Table 2). While these shift assignments must at present remain somewhat tentative,[38] it is encouraging to note that Bart et al.[39] identified the H_2 signal in solution by ^{2}H NMR on a sample selectively ^{2}H-labeled on the α-imine methyl. This enabled us to determine the corresponding ^{13}C (C_2) shift by recording an HMQC on the sample at natural abundance (see Supporting Information), dissolved in dichloromethane. Both ^{1}H and ^{13}C shifts match closely the values measured and assigned in the solid-state spectrum. Moreover, the C_2H_2 cross-peak in a TEDOR spectrum of the corresponding methyl-d_6 labeled species was absent. Relaxation data could also in principle further assist in the assignment process, as the paramagnetic relaxation enhancement depends on the distance between observed nuclei and the paramagnetic center, and significant variations in T_1 and T_2' enhancements could indeed be observed for the different nuclear sites in the iron complex. However, the interpretation of these effects in the presence of a highly delocalized electronic spin density is not straightforward. In addition, a more complete model for the paramagnetic relaxation in solids under MAS may be required for interpreting the enhancements.

Electronic Structure. Molecular orbital (MO) analyses of the calculated wave functions provide a graphical representation of the spin-density distribution in **1**. As shown in Figure 6b−e for α_{HOMO}, α_{HOMO-1}, α_{HOMO-2}, and α_{HOMO-5}, the frontier metal 3d orbitals associated with the four unpaired electrons are d_{xy}, d_{z^2}, d_{xz}, and d_{yz}. The $d_{x^2-y^2}$ is however doubly occupied and appears as β_{HOMO} (Figure 6f). So the 3d orbital configuration in this metal complex is $(d_{x^2-y^2})^2(d_{yz})^1(d_{xz})^1(d_{z^2})^1(d_{xy})^1$. A comparison with the contour plot of the spin density shows that clearly most of the spin density is localized primarily in the d_{xz} orbital and that here only two lobes of d_{xy} (α_{HOMO}) interact with the ligand in the plane (Figure 6b) and that $d_{xz/yz}$ have little interaction with this ligand in **1** (Figures 6d,e). This probably explains the smaller chemical shift windows observed for **1** compared to these reported for deoxy myoglobin (up to ∼800 ppm), also an Fe^{II} molecular system having the spin state $S = 2$, but a $(d_{xy})^2(d_{yz})^1(d_{xz})^1(d_{z^2})^1(d_{x^2-y^2})^1$ configuration, as a result of different structural symmetries and ligand interactions.[33] This shows once more how NMR allows direct, straightforward experimental access to the fine details of the molecular electronic configuration, which is in turn a sensible reporter of the molecular geometry. It has been nicely demonstrated that the catalytic reactivity of the diimine−iron complex family is correlated with the metal spin state and can be carefully tuned by the choice of the ligand substituents.[20] The ability to evaluate hyperfine shifts in paramagnetic complexes offered by quantum chemical methods can therefore open new perspectives where the calculation and the refinement of a structure, and the prediction of its reactivity, are accomplished using NMR hyperfine data as a structural probe.

Conclusions

We have shown a protocol for the complete structural characterization of paramagnetic molecular powders at natural abundance by solid-state NMR. The approach was successfully demonstrated on an organometallic catalyst based on high-spin Fe^{II}.

The combination of very fast MAS and of broadband TEDOR recoupling allows the observation of 2D heteronuclear correlations. These spectra provide a tool for removing the correlated inhomogeneous broadening, can be acquired over a remarkably short experimental time, and record almost all the proton and carbon signals expected from the ligand spins with high sensitivity and good resolution.

The efficient detection of NMR signals in highly paramagnetic molecules provides easy access to the structural features of the environment of a paramagnetic center, which in turn possess a strong, straightforward relationship with the fine details of the electronic state of the system. A complete assignment of the observed resonances was possible by coupling spectral editing measurements to hybrid density functional theory calculations, which enabled accessing the metal wave functions and reproducing the NMR experimental data based on the known crystal structure of the complex.

The present work therefore delineates a new role for NMR in combination with DFT, in studies where NMR hyperfine observables may be exploited as structural probes closer to a paramagnetic center, for possibly exploring the nature and the reactivity of catalytically active species and for driving the design of new active complexes. We believe that the solid-state NMR analysis of paramagnetic powders will feature strategic applications for the understanding of solid-state reactions, as already shown for surface diamagnetic catalysts,[2] and will strongly contribute to the development of supramolecular, nanoscale, and surface chemistry.

Experimental Section

Sample Preparations. The Fe^{II} complex **1** was prepared using the literature procedure.[39]

Preparation of 2,3-Dimethyl-1,4-[(2′,6′)-diisopropylphenyl]-*N*,*N*′-diazadiene Zinc Dichloride (2). Using the procedure described by Sandrini et al.,[40] a mixture of 2,3-dimethyl-1,4-[(2′,6′)-diisopropylphenyl]-*N*,*N*′-diazadiene[19] (0.620 g, 1.53 mmol) in THF (10 mL) was added to $ZnCl_2$ (0.189 g, 1.39 mmol) in THF (5 mL) at 25 °C. After a few minutes, a precipitate was formed, and the reaction mixture was stirred for an additionnal 2 h and then filtered. The resulting solid was washed with THF and pentane and then dried under a high vacuum (10^{-6} Torr)

to give 0.685 g of **2** (91.1%). ^{1}H NMR ($CDCl_3$): $\delta = 1.13$ (d, $J = 6.84$ Hz, 12H, **CH*Me*$_2$**), 1.33 (d, $J = 6.84$ Hz, 12H, **CH*Me*$_2$**), 2.35 (s, 6H, **N=C−C*H*$_3$**), 2.9 (sept, $J = 6.84$ Hz, 4H, **C*H*Me$_2$**), 7.3 (m, 6H, **C*H*$_{Ar}$**). ^{13}C NMR ($CDCl_3$): $\delta = 20.2$ (***C*$_9$**), 24 (***C*$_{10}$−**11**), 28.74 (***C*$_2$**), 124.67 (***C*$_6$**), 128.11 (***C*$_7$**), 139.08 (***C*$_8$**), 150 (N***C*$_3$**), 170 (***C*$_1$**). Elemental analysis for **2** [$C_{28}H_{40}N_2Cl_2Zn$] Calculated: C, 63.84%$_{wt}$; N, 5.32%$_{wt}$; Cl, 13.46%$_{wt}$; Zn, 12.41%$_{wt}$. Found: C, 62.33%$_{wt}$; N, 5.34%$_{wt}$; Cl, 13.10%$_{wt}$; Zn, 12.87%$_{wt}$.

NMR Spectroscopy. Samples for NMR spectroscopy were prepared by packing approximately 5 mg of powder under argon into a 2.5 mm zirconia rotor, which was sealed by simply tightly closing the rotor cap.

All solid-state NMR spectra were acquired on a Bruker Avance-500 spectrometer operating at a proton frequency of 500 MHz and equipped with a double-resonance 2.5 mm CP-MAS probe. Experimental ^{13}C and ^{1}H shifts were referenced to TMS at 0 ppm using an external standard of glycine, with the methyl signal at 19.8 and 1.18 ppm for ^{13}C and ^{1}H, respectively. Sample temperature was kept constant to a value of 30 ± 0.5 °C.

In a typical experiment, the lengths of the 90° ^{1}H and ^{13}C pulses were about 1.5 and 2.5 μs, respectively. In a CP sequence, a tangential amplitude modulated RF field[41] centered at 100 kHz was applied on ^{1}H, while the carbon field on ^{13}C was matched to obtain an optimal signal; at spinning speeds of about 30 kHz, an optimal contact time was found around 500 μs for all the signals. TEDOR (transferred-echo, double resonance) experiments were performed according to a standard pulse sequence (see, e.g., ref 25, together with the phase cycle reported in Table 1 therein); the optimal recoupling time was equal to 2 rotational periods τ_R. Improvements in sensitivity could be obtained by a modified version of the experiment, as shown in Figure 2c and in the Supporting Information, where the z-filter element at the end of the sequence is removed and the acquisition starts directly at the last recoupling period.

As fast MAS efficiently removes a large part of the ^{1}H−^{13}C dipolar couplings as well as ^{1}H−^{1}H dipolar couplings, *neither heteronuclear nor homonuclear decoupling was applied during acquisition*.[9] In all the ^{1}H and ^{13}C spectra, the signals were recorded with down to 2 μs sampling and for a total acquisition time of 2 and 32 ms, respectively. To avoid baseline distortions on the very large spectral width, a rotor-synchronous spin−echo sequence was always used before acquisition. The spin−echo block is turned into a REDOR-type recoupling sequence if two 180° pulses are applied on the ^{1}H channel in the center of each echo delay, so that the ^{1}H−^{13}C dipolar couplings are reintroduced during the echo evolution.[31,32]

Nonrefocusable transverse (T_2') and longitudinal (T_1) relaxation times were measured, respectively, with standard rotor-synchronized spin−echo and inversion−recovery methods.

2D ^{1}H−^{13}C heteronuclear dipolar correlation (HETCOR) spectra were recorded with either the CP or the TEDOR schemes, and with rotor-synchronization of the t_1 increments. In both cases, a total of 16 to 32 t_1 increments were collected ($t_{1max} = 0.33$ ms; $t_{2max} = 32.7$ ms), with 16k to 50k scans each and a recycle delay of 0.1 s (total recording time 7 to 28 h). Quadrature detection during f_1 was achieved using the States method. An exponential line broadening of 100 Hz was applied in the two dimensions before Fourier transformation.

Single-Crystal X-ray Structure Determination. Crystal data and details of the structure determination are presented in Table 1. Suitable single-crystals for the X-ray diffraction study were grown with standard cooling techniques. The selected crystal was stored under perfluorinated ether, transferred in a Lindemann capillary, fixed, and sealed. Preliminary examination and data collection were carried out on an area detecting system (NONIUS, MACH3, κ-CCD) at the window of a rotating anode (NONIUS, FR591) and graphite-monochromated Mo Kα radiation ($\lambda = 0.710\ 73$ Å). The unit cell parameters were obtained by full-matrix least-squares refinements during the scaling procedure with 2939 reflections. Data collection was performed at $T = 173$ K (OXFORD CRYOSYSTEMS). Nine data sets were measured in rotation scan modus with $\Delta\varphi/\Delta\omega = 1.0$. Intensities were integrated, and the raw data were corrected for Lorentz and polarization and, arising from the scaling procedure, for latent decay and absorption effects. The structures was solved by a combination of direct methods and difference Fourier syntheses. All non-hydrogen atoms were refined with anisotropic displacement parameters. All hydrogen atoms were located from difference Fourier maps and were allowed to refine freely. Full-matrix least-squares refinements were carried out by minimizing $\Sigma w(F_o^2 - F_c^2)^2$ with the SHELXL-97 weighting scheme and stopped at shift/err < 0.001. The final residual electron density maps showed no remarkable features (+0.32/−0.24 eÅ^{-3}). Neutral atom scattering factors for all atoms and anomalous dispersion corrections for the non-hydrogen atoms were taken from *International Tables for Crystallography.* All calculations were performed on an Intel Pentium II PC, with the STRUX-V system, including the programs PLATON, SIR92, and SHELXL-97.[42] Crystallographic data (excluding structure factors) for the structure reported in this paper have been deposited with the Cambridge Crystallographic Data Centre as supplementary publication no. CCDC-620797 (**1**). Copies of the data can be obtained free of charge on application to CCDC, 12 Union Road, Cambridge CB2 1EZ, UK (fax: (+44)1223−336−033; e-mail: deposit@ccdc.cam.ac.uk).

DFT Calculations. The calculations of solid-state NMR Fermi-contact hyperfine shifts and diamagnetic chemical shifts of complex **1** were performed with the hybrid Hartree−Fock density functional theory (HF-DFT) method B3LYP[43] in the Gaussian 03 program,[44] on its X-ray structure without further manipulation, as we did before for other systems.[34] A large basis set scheme was used (an all-electron Wachters' basis (62111111/3311111/3111) for Fe,[45] 6-311G* for other heavy atoms, and 6-31G* for hydrogen atoms), as previously reported for the evaluation of the hyperfine properties for paramagnetic complexes of different transition metals (Fe, Mn, Cu, V, Ag).[33−35] Once the contribution from the bulk magnetic susceptibility is removed, the total shift δ_{obs} (eq 1) is evaluated by calculating the diamagnetic contribution (δ_{dia}) and the Fermi contact (δ_{FC}) term; contributions from the pseudocontact term (δ_{pc}) are neglected in the calculations.[33−34,46] The quantum chemical methods allow the direct evaluation of the spin density $\rho_\alpha\beta$ of a nucleus of interest, which enables in turn the prediction of δ_{FC} as

$$\delta_{FC} = m(S+1)\rho_\alpha\beta/T \qquad (2)$$

where S is the spin state of the system, T is the temperature, and m is a collection of physical constants and is equal to 2.35×10^7 ppm K au^{-1}.[33,34]

Acknowledgment. We thank D. Gajan and N. Delpont for their participation in this study as a part of their undergraduate project and P. J. Chirik for providing d_6-**1**, and J. Sachleben for fruitful discussions. We are grateful to IDECAT, CNRS, CPE Lyon, and ENS Lyon for financial support. E.O. and Y.Z. were supported by NIH Grant GM50694. NMR spectra were recorded at the Rhône-Alpes Large Scale Facility for NMR.

Supporting Information Available: Complete ORTEP plot, tables of crystallographic data, atomic coordinates, atomic displacement parameters, bond distances, and bond angles for complex **1**; complete ref 44; MAS NMR spectra used to assign the diamagnetic analogue **2** (^{1}H−^{13}C dipolar HETCOR and ^{1}H DQ CRAMPS correlations); comparison between different versions of TEDOR sequences; correlation betweeen experimental shifts for complex **2** and calculated diamagnetic shifts for **1**; 1D ^{1}H and 2D ^{1}H,^{13}C-HMQC spectra of **1** dissolved in CD_2Cl_2. This material is available free of charge via the Internet at http://pubs.acs.org.

JA063510N